Resonant mixing in perturbed action-action-angle flow

Dmitri L. Vainchtein
School of Physics, Georgia Institute of Technology, Atlanta, Georgia 30332, USA and Space Research Institute, Moscow, Russia

John Widloski and Roman O. Grigoriev
School of Physics, Georgia Institute of Technology, Atlanta, Georgia 30332, USA
(Received 21 February 2008; published 5 August 2008)

This paper presents a quantitative theory of mixing via chaotic advection in near-integrable time-dependent volume-preserving flows for the case when the base (unperturbed) flow possesses two invariants (or actions). Using a model cellular flow introduced by Solomon and Mezic as an example, we construct a quantitative theory of mixing caused by the resonance-induced diffusion of an adiabatic invariant of the flow. We compute the fraction of the mixed volume as a function of the frequency of the perturbation and show that this function is strikingly nonmonotonic, with multiple peaks. In particular, essentially complete mixing inside a flow cell is achieved on experimentally accessible time scales for certain special frequencies.

DOI: 10.1103/PhysRevE.78.026302 PACS number(s): 47.51.+a, 47.61.Ne, 47.52.+j

I. INTRODUCTION

In the context of fluidic systems, mixing is conventionally identified with homogenization of any initially localized distribution of passive tracers throughout the cross section (for open flows) or volume (for bounded flows) of the fluid. Although this is similar to the more technical definition of the term in the context of ergodic theory, where it describes the evolution of phase space volumes, we will accept a less formal definition motivated by applications to experiment. Specifically, we will use the term *mixing* to describe the broadening of the distribution of passive tracers advected by the flow in such a way that it asymptotically (or after a sufficiently long time) disperses over a subset of the fluid volume, covering it completely except for holes of size smaller than some cutoff δ. In this way, one can define mixing to be one, two, or three dimensional, depending on the dimensionality of the subset. The cutoff δ can be interpreted as either the resolution of an experimental measurement or an effective length scale below which molecular diffusion becomes the dominant transport mechanism.

Weakly perturbed volume-preserving action-action-angle flows (which possess two invariants in the absence of a perturbation) have a special place in the studies of Lagrangian mixing. On the one hand, such flows arise frequently in microfluidic devices where geometric symmetries severely constrain the flow structure, leading to the emergence of multiple flow invariants (or actions). On the other hand, an arbitrarily small perturbation can completely break the integrability of such a flow, enabling essentially complete mixing [1], unlike action-angle-angle flows in which surviving Kolmogorov-Arnold-Moser- (KAM-)like regular tori impede global transport, leading to poor mixing.

Mixing in action-action-angle flows in the presence of time-*independent* perturbations is already quite well understood. However, for time-periodic perturbations, only qualitative descriptions of the mixing process were available until now. In fact, two rather different mechanisms have been proposed to explain mixing.

The first study of this problem is due to Feingold and co-workers [2,3], who recognized that mixing is caused by the breakdown of adiabatic invariance (the latter arising due to averaging over fast time scales) near surfaces where the frequency of the perturbation is in resonance with the frequency of the unperturbed (base) flow. The resulting dynamics was described as a combination of segments of adiabatic motion away from resonance surfaces combined with segments of nonadiabatic motion near resonance surfaces. The assumption of the randomness of the jump in the value of the adiabatic invariant associated with the crossing of the resonance surface was used to argue a gradual dispersion in the value of the adiabatic invariant, leading to mixing. However, the jump magnitude was not computed nor was the assumption of randomness in the jump direction justified.

This qualitative theory of resonance-induced dispersion or diffusion was later applied to a model of fluid flow between concentric spheres rotating about different axes [1,4], where it was discovered that, for some parameters and on very long time scales, essentially complete mixing can be achieved due to a special property of the flow—its resonance surfaces are dense in the whole volume between the spheres.

The first attempt to achieve a more detailed understanding of the effect of resonances was made by Mezic [5], who suggested that the dynamics near resonance surfaces is governed by the hyperbolic saddle and saddle-focus periodic orbits, surviving in the presence of the perturbation, and their heteroclinic connections. Specifically, it was proposed that changes in the value of the adiabatic invariant are mainly associated with passages through the neighborhoods of saddle-focus-type periodic orbits, whose stable and unstable manifolds are inclined with respect to the resonance surface. However, again, no quantitative theory describing the change in the value of the adiabatic invariant was constructed.

Following these theoretical studies, several experimental and numerical investigations of Lagrangian mixing in time-periodic flows were undertaken. These investigations discovered that the mixing efficiency exhibits a nonmonotonic dependence on the frequency of the time-periodic component of the flow. Qualitatively similar results were obtained in the presence of molecular diffusion [6,7] as well as without it [8–10], suggesting that molecular diffusion likely does not play a significant role in this phenomenon.

Finally, a quantitative theory of resonance-induced adiabatic diffusion was developed in Ref. [11] for time-independent perturbations. The generalization of this theory for time-periodic perturbations was summarized in Ref. [12], along with an explanation of the observed nonmonotonic frequency dependence of the mixing efficiency. The latter study was based on the theory of resonance phenomena in multiple-frequency systems developed recently by Neishtadt [13]. The purpose of this paper is to present a more detailed description of the dynamics in the vicinity of resonance surfaces that underlies the quantitative theory of mixing in near-integrable time-dependent volume-preserving flows.

The paper is organized as follows. We start in Sec. II by introducing the model flow. Section III describes the adiabatic motion far from resonances. Different types of dynamics near the resonance surface(s) are described in Sec. IV. The cumulative effect of many resonance crossings on the dynamics of the adiabatic invariant and the consequences for mixing are considered in Sec. V. Finally, Sec. VI presents the summary and conclusions.

II. THE MODEL FLOW

To illustrate the effect of resonances on the mixing dynamics, we consider an incompressible fluid flow in a one-dimensional array of cubic cells described by the following equations:

$$\dot{x} = v_x = -\cos(\pi x_s)\sin(\pi y) + \varepsilon \sin(2\pi x_s)\sin(\pi z),$$

$$\dot{y} = v_y = \sin(\pi x_s)\cos(\pi y) + \varepsilon \sin(2\pi y)\sin(\pi z),$$

$$\dot{z} = v_z = 2\varepsilon \cos(\pi z)[\cos(2\pi x_s) + \cos(2\pi y)], \tag{1}$$

where $x_s = x + b \sin \omega t$. This system was introduced by Solomon and Mezic in [10] as a qualitative model of a Lorenz-force-driven cellular flow in a channel of rectangular cross section $(-0.5 < y, z < 0.5)$. It is easy to check that the no-slip boundary condition at the channel walls is not satisfied. However, we point out that using the exact solution of the Navier-Stokes equations satisfying the proper boundary conditions will lead us to qualitatively the same conclusions while making the calculations unnecessarily complicated.

The terms proportional to ε describe a weak correction to the main recirculation flow caused by inertial effects (Eckman pumping). The time dependence of the flow is due to an external perturbation—the shift, with amplitude b, of the boundaries between the cells (planes $x = n + 1/2$, $n \in Z$). For nonzero b, there is transport between the cells; however, our objective is to understand the transport properties of the flow inside each of the cells. Since the dynamics in all the cells is identical, we will consider only the cell with $-0.5 < x < 0.5$.

Following [10], we consider the limit $0 \le \varepsilon \ll 1$ and $0 \le b \ll 1$. Linearizing (1) with respect to ε and b, we obtain a time-periodic near-integrable flow

$$\dot{x} = -\cos(\pi x)\sin(\pi y) + \pi b \sin(\pi x)\sin(\pi y)\sin \omega t + \varepsilon \sin(2\pi x)\sin(\pi z),$$

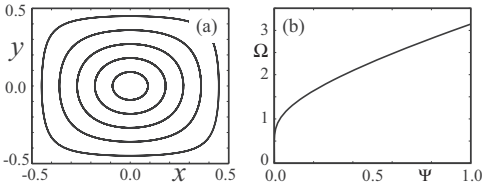

FIG. 1. Unperturbed system: (a) typical streamlines in the z =const plane and (b) the frequency $\Omega(\Psi)$.

$$\dot{y} = \sin(\pi x)\cos(\pi y) + \pi b \cos(\pi x)\cos(\pi y)\sin \omega t + \varepsilon \sin(2\pi y)\sin(\pi z),$$

$$\dot{z} = 2\varepsilon \cos(\pi z)[\cos(2\pi x) + \cos(2\pi y)], \tag{2}$$

which can be analyzed using perturbative techniques.

III. ADIABATIC MOTION

In this section we describe the dynamics far from the resonance surfaces. Our main objective in the present section is to derive the averaged equations of motion and show that, for small b and ε, the dynamics conserves an adiabatic (approximate) invariant, restricting transport to two dimensions.

A. Unperturbed flow

First, consider the unperturbed (base) flow characterized by $\varepsilon = 0$ and $b = 0$. In this case, $x_s = x$ and (1) is reduced to

$$\dot{x} = -\cos(\pi x)\sin(\pi y),$$

$$\dot{y} = \sin(\pi x)\cos(\pi y),$$

$$\dot{z} = 0. \tag{3}$$

This is a two-dimensional autonomous flow which possesses two invariants (actions, integrals of motion):

$$z = \text{const},$$

$$\Psi = \cos(\pi x)\cos(\pi y) = \text{const}, \tag{4}$$

with Ψ proportional to the stream function of the unperturbed flow in the (x, y) plane. All the streamlines $\Gamma_{z,\Psi}$ of the unperturbed flow are closed, except for those residing on the cell boundaries [see Fig. 1(a)], with the period of motion

$$T(\Psi) = 2\int_{x_{\min}}^{x_{\max}} \frac{1}{\dot{x}} dx = 4\int_0^{x_{\max}} \frac{dx}{\sqrt{\cos^2(\pi x) - \Psi^2}}, \tag{5}$$

where $x_{\max} = -x_{\min} = (1/\pi)\cos^{-1}\Psi$. The corresponding frequency $\Omega = 2\pi/T$ is shown in Fig. 1(b) and ranges from $\Omega = 0$ on the cell boundaries to $\Omega = \pi$ at the center. On every $\Gamma_{z,\Psi}$ we can introduce a uniform phase, χ mod(2π), such that $\chi = 0$ on the positive x axis and

$$\dot{\chi} = \Omega(\Psi). \tag{6}$$

The base flow (3) can therefore be rewritten as a system of Eqs. (4) and (6), explicitly illustrating that it is of the action-

action-angle type. The actions Ψ, z, and the angle χ provide a convenient set of coordinates that parametrize all interior points of the flow cell.

The unperturbed flow is characterized by mixing in only one dimension (along the streamlines $\Gamma_{z,\Psi}$). Using (5) and (6) we find that an initial tracer distribution of finite width will get stretched along $\Gamma_{z,\Psi}$ at a rate $O(1)$, eventually becoming uniform over the whole streamline.

B. Time-independent perturbation

Next, consider the effect of the Eckman pumping ($\varepsilon > 0$), ignoring the time-dependent shift for the moment ($b=0$). In this limit, the flow (2) is steady but conserves neither z nor Ψ. The dynamics is characterized by two different time scales: the variable χ is fast [changes on $O(1)$ time scale], while the variables z and Ψ are slow [change on $O(\varepsilon^{-1})$ time scale].

The evolution equations for the slow variables follow directly from (2). Specifically,

$$\dot{\Psi} = -2\pi\varepsilon \sin(\pi z)\Psi[\sin^2(\pi x) + \sin^2(\pi y)],$$

and the equation for $\dot{z}$ is unchanged. Averaging these over the quick oscillations in χ over one period of the unperturbed motion, we obtain the following dynamics:

$$\dot{\Psi} = -\varepsilon\frac{16\pi}{T(\Psi)}\sin(\pi z)\Psi\int_0^{x_{\max}}\frac{\sin^2(\pi x)}{\sqrt{\cos^2(\pi x) - \Psi^2}}dx,$$

$$\dot{z} = \varepsilon\frac{16}{T(\Psi)}\cos(\pi z)\int_0^{x_{\max}}\frac{\cos(2\pi x)}{\sqrt{\cos^2(\pi x) - \Psi^2}}dx. \tag{7}$$

It can be shown [14] that the averaged (slow) system (7) possesses a new integral of motion: the flux Φ of the vector field

$$\mathbf{v}_\varepsilon = \begin{pmatrix} \sin(2\pi x)\sin(\pi z) \\ \sin(2\pi y)\sin(\pi z) \\ 2\cos(\pi z)[\cos(2\pi x) + \cos(2\pi y)] \end{pmatrix},$$

the ε-dependent part of the perturbation in (2), through a surface S_Γ bounded by an unperturbed streamline $\Gamma_{z,\Psi}$. Specifically, we have

$$\Phi = \int_{S_\Gamma}(\mathbf{v}_\varepsilon \cdot \mathbf{n})dS, \tag{8}$$

where $\mathbf{n}$ and dS are the unit normal vector and the surface element on S_Γ, respectively. Using a vector potential

$$\mathbf{A}_\varepsilon = \begin{pmatrix} A_x \\ A_y \\ A_z \end{pmatrix} = \frac{1}{\pi}\cos(\pi z)\begin{pmatrix} -\sin(2\pi y) \\ \sin(2\pi x) \\ 0 \end{pmatrix}, \tag{9}$$

such that $\mathbf{v}_\varepsilon = \nabla \times \mathbf{A}_\varepsilon$, we can rewrite (8) as

$$\Phi = \oint_{\Gamma_{z,\Psi}}(\mathbf{A}_\varepsilon \cdot d\mathbf{l}), \tag{10}$$

where $d\mathbf{l}$ is a length element on $\Gamma_{z,\Psi}$. Substituting (9) into (10), we get

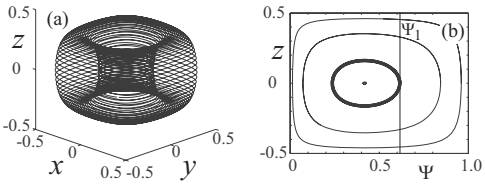

FIG. 2. Autonomous perturbed system ($\varepsilon = 10^{-4}, b=0$): (a) Quasiperiodic motion in the physical space; (b) The projection on the slow plane. The vertical line shows the location of the 1:1 resonance (for $b \neq 0$ and $\omega = 2.5$) and the bold curve is Γ_{Φ^*} (see Sec. V B)

$$\begin{aligned}\Phi &= \oint_{\Gamma_{z,\Psi}}(A_x dx + A_y dy) \\ &= \frac{2}{\pi}\cos(\pi z)\Psi\int_0^T[\sin^2(\pi x) + \sin^2(\pi y)]dt \\ &= \frac{16}{\pi}\cos(\pi z)\int_0^{x_{\max}}\frac{\Psi}{\cos(\pi x)}\sqrt{1 - \frac{\Psi^2}{\cos^2(\pi x)}}dx. \end{aligned} \tag{11}$$

One can see that (7) can be written as

$$\dot{\Psi} = -\varepsilon\frac{\pi}{T(\Psi)}\frac{\partial\Phi}{\partial z}, \quad \dot{z} = \varepsilon\frac{\pi}{T(\Psi)}\frac{\partial\Phi}{\partial\Psi}. \tag{12}$$

Therefore, Φ is an invariant of the averaged system and, hence, is an adiabatic invariant (AI) of the exact system: far from the cell boundaries, where $\Omega(\Psi)=0$, the value of Φ oscillates with an amplitude $O(\varepsilon)$, but on any one *full* turn of the fast motion the change in Φ is only $O(\varepsilon^2)$, compared with $O(\varepsilon)$ changes in Ψ and z [13]. Therefore, on time intervals $O(\varepsilon^{-1})$, Ψ and z experience an $O(1)$ change, while Φ only changes by $O(\varepsilon)$. For a detailed proof that Φ is an AI, see [14].

In the physical space, the streamlines of the flow with $b=0$ lie on the nested tori τ_Φ [see Fig. 2(a)] defined as the level sets of the AI. The (quasiperiodic) motion along these tori corresponds to motion, with slow period $T_\varepsilon(\Phi)$, of the averaged system (12) along the closed curves Γ_Φ on the (Ψ, z) plane [see Fig. 2(b)]. In the physical space, the AI reaches its maximum value $\Phi_c \approx 0.7845$ on a closed curve that resides in the center of the nested tori and is given by

$$z = z_c = 0, \quad \Psi = \Psi_c \approx 0.418. \tag{13}$$

It follows from (7) that $\dot{z}$ can be written in terms of a complete elliptic function of Ψ, with Ψ_c being its only zero for $-0.5 < z < 0.5$ (see, e.g., [15]). Also, one can find that $\dot{z}$ is negative for $\Psi < \Psi_c$ and positive for $\Psi > \Psi_c$. Therefore, all trajectories in the slow plane move around the point (Ψ_c, z_c) in a counterclockwise direction [Fig. 2(b)].

The steady perturbed flow is characterized by mixing in two dimensions (along a level set $\tau_{\Phi(z,\Psi)}$). In addition to the fast stretching along $\Gamma_{z,\Psi}$ described previously, the tracer distribution will also be stretched in the direction normal to $\Gamma_{z,\Psi}$ at a slower rate [more specifically, $O(\varepsilon)$, according to (12)], eventually becoming uniform over the whole level set.

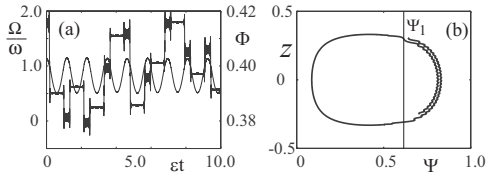

FIG. 3. Complete flow with $\varepsilon=b=10^{-4}$ and $\omega=2.5$: (a) Plots of Ω/ω (dashed line) and Φ (solid line) vs time for complete flow (1); (b) projection of one slow period on the slow plane, the 1:1 resonance is shown.

C. Time-dependent perturbation

The addition of the time-dependent perturbation can make the structure of the flow much more complex. Numerical simulations show that the limit $0<b\ll\varepsilon$ is qualitatively similar to the case with $b=0$ and $\varepsilon>0$.

The limit $0<\varepsilon\ll b$ is qualitatively similar to the case with $\varepsilon=0$ and $b>0$, where the flow is effectively two dimensional and a narrow chaotic layer of width $O(b)$ appears near the cell boundaries. While this layer has little influence on transport inside any one cell, it plays a key role in the intercell transport. As these layers from the adjacent cells are connected, their existence opens the possibility of Lévy-flight-like transport across many cells (see [16,17]).

The case where b and ε are of similar magnitude is of the most interest for transport inside cells. Hence, in what follows we assume $\beta\equiv b/\varepsilon=O(1)$. Furthermore, since we are interested in the dependence of mixing properties of the flow on the frequency ω of the perturbation, we will also assume $\omega=O(\Omega)=O(1)$.

The evolution equations for the slow variables are now

$$\dot{\Psi}=-2\pi\varepsilon\sin(\pi z)\Psi[\sin^2(\pi x)+\sin^2(\pi y)]-\frac{1}{2}\varepsilon\pi^2\beta[\sin(2\pi y)\sin(\omega t)],$$

$$\dot{z}=2\varepsilon\cos(\pi z)[\cos(2\pi x)+\cos(2\pi y)]. \tag{14}$$

If Ω and ω are incommensurate, then averaging over χ and t can be performed independently (see, e.g., [13]). In this case, the time-dependent terms in the equation for $\dot{\Psi}$ average out and we would expect the AI (11) to be conserved as before. The evolution over a longer time interval shows that the AI remains essentially constant except for the short periods of time when $\Omega\approx\omega$, as Fig. 3 illustrates. We therefore find, as previous studies [1–4] did, a clear indication of the fact that the breakdown of adiabatic invariance is a consequence of processes occurring in the vicinity of resonances.

IV. RESONANT PHENOMENA

In this section we develop a quantitative description of the dynamics near resonance surfaces based on the theory of resonance phenomena in multiple-frequency systems [13]. The primary goal of this description is to compute the magnitude of the jump experienced by the AI upon crossing a resonance surface.

As the value of Ψ slowly drifts, so does $\Omega(\Psi)$. Hence, at certain values of Ψ a resonance condition

$$n\Omega(\Psi)-\omega=0 \tag{15}$$

will be satisfied for some nonzero integer n. Note that (15) is a special case of a more general resonance condition $n\Omega=m\omega$ which corresponds to a generic time-periodic perturbation. The restriction to $m=1$ in our case is a consequence of the particular form of the time-dependent perturbation in (2), namely, that only the first harmonic is present. Since Ω is independent of z, all resonance surfaces R_n, defined by $\Psi(x,y)=\Psi_n\equiv\Omega^{-1}(\omega/n)$, are vertical cylinders in the physical space or vertical lines $\Psi=\Psi_n$ in the slow plane [see Fig. 2(b)].

Near R_n, we can expect neither the averaged system to adequately describe the exact dynamics, nor the value of Φ to be conserved. Hence, we must consider the dynamics near resonances separately. Unlike autonomous systems with resonance phenomena (see, e.g., Ref. [11]), where the fast (unperturbed) dynamics slows down near a resonance, for the flow studied here both the fast angle variable χ and the phase of the perturbation ωt keep changing rapidly. It is only a particular linear combination of these phases that slows down:

$$\gamma=n\chi-\omega t.$$

Therefore, near every resonance surface there is just one independent fast variable, χ, rather than two far from the resonances. Of the three other variables, Ψ [or $\Omega(\Psi)$] and z are slow and γ is semislow, with characteristic rates of change of order $O(\varepsilon)$ and $O(\varepsilon^{1/2})$, respectively. We can still average the exact equations of motion for all the slow and semislow variables over χ (perform the so-called *partial averaging*; see [13]) in order to obtain the equations of motion near a resonance surface:

$$\gamma'=\frac{1}{\sqrt{\varepsilon}}(n\Omega-\omega),$$

$$\Omega'=\sqrt{\varepsilon}\frac{\partial\Omega}{\partial\Psi}\frac{\dot{\Psi}}{\varepsilon},$$

$$z'=\sqrt{\varepsilon}\frac{\dot{z}}{\varepsilon}. \tag{16}$$

In (16), the prime denotes the derivative with respect to the rescaled time $\bar{t}=\sqrt{\varepsilon}t$ and $\dot{\Psi},\dot{z}$ were defined in (14).

A. Scattering on resonance

For most initial conditions, tracers pass through the vicinity of resonance in a relatively short time and the value of Φ undergoes a relatively small change. In the first approximation we can fix the value of slow variables Ω and z at the resonance values, which yields a forced-pendulum-like equation for γ:

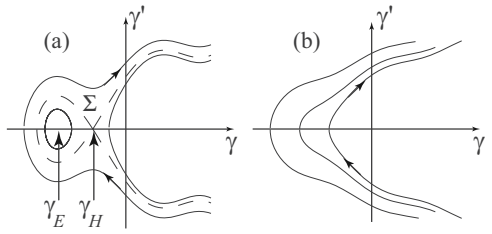

FIG. 4. Schematic phase portraits on the (γ,γ') plane. The dashed line shows the separatrix Σ of the hyperbolic fixed point $(\gamma_H,0)$; Σ encloses the elliptic fixed point $(\gamma_E,0)$.

$$\gamma' = \frac{1}{\sqrt{\varepsilon}} n\Omega' = a_n + b_n \cos\ \gamma, \tag{17}$$

where the coefficients a_n and b_n correspond to the averages of the first and the second term, respectively, in the expression for $\dot{\Psi}$ in (14) over the fast period $T_n \equiv T(\Psi_n) = 2\pi n/\omega$:

$$a_n = -n\Psi\ \sin(\pi z_*)\frac{\partial\Omega}{\partial\Psi}\int_0^{2\pi}[\sin^2(\pi x) + \sin^2(\pi y)]d\chi,$$

$$b_n = -\frac{\pi}{4} n\beta\frac{\partial\Omega}{\partial\Psi}\int_0^{2\pi}\sin(2\pi y)\sin(n\chi)d\chi, \tag{18}$$

and the asterisk denotes the value of z at which the crossing occurs (see Appendix A for details).

The relative magnitude of a_n and b_n defines the structure of the phase portrait describing the dynamics in the (γ,γ') plane. The phase portrait for the case $|b_n| > |a_n|$ is shown in Fig. 4(a) for one period of γ. The phase portrait for the case $|b_n| < |a_n|$ is shown in Fig. 4(b). As presented, Fig. 4 corresponds to $a > 0$. For $a < 0$, the phase portraits would be reflected with respect to the vertical axis and the direction of the flow would be reversed. We should point out that the relative magnitude of a_n and b_n depends on the values of ω, β, and Φ and is independent of ε.

The average of $\dot{\Phi}$ over one fast period T_n can be computed using (12) and (14), yielding

$$\langle\dot{\Phi}\rangle_{T_n} = \left\langle \frac{\partial\Phi}{\partial\Psi}\frac{d\Psi}{dt} + \frac{\partial\Phi}{\partial z}\frac{dz}{dt}\right\rangle_{T_n}$$

$$= -\frac{\pi^2}{2}\beta\langle\dot{z}\ \sin(2\pi y)\sin(\omega t)\rangle_{T_n}$$

$$= \varepsilon\pi\beta c_n\cos(\pi z_*)\cos\ \gamma, \tag{19}$$

where the coefficient c_n is given by

$$c_n = -\frac{n}{\omega}\int_0^{2\pi}[\cos(2\pi x) + \cos(2\pi y)]\sin(2\pi y)\sin(n\chi)d\chi.$$

Now the jump of the AI on crossing the resonance can be computed as a change in Φ over a time interval (t_1,t_2) during which the resonance is crossed once, at time t_*, such that $|t_{1,2} - t_*| = O(\varepsilon^{-1})$. To the leading order,

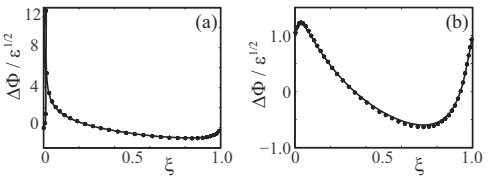

FIG. 5. Change in the AI on crossing the 1:1 resonance as a function of ξ for $z_* = 0.35$, $\omega = 2.5$ with $\beta =$ (a) 1 and (b) 0.5. The solid lines correspond to the theoretical value (21) and the asterisks show the values obtained by numerical integration of (1) with $\varepsilon = 10^{-4}$. Note the singularity at $\xi_{\text{sing}} \approx 0.02$ in (a) associated with close passages by the hyperbolic fixed point $(\gamma_H,0)$ not resulting in captures.

$$\Delta\Phi = \int_{t_1}^{t_2}\langle\dot{\Phi}\rangle dt = -2\sqrt{\varepsilon}s\pi\beta\cos(\pi z_*)c_n$$

$$\times\int_{-s\infty}^{\gamma(t_*)}\frac{\cos\ \gamma}{\sqrt{2(V_* - V)}}d\gamma + O(\varepsilon). \tag{20}$$

where $V(\gamma) \equiv -a_n\gamma - b_n\sin\ \gamma$, $V_* \equiv V(\gamma(t_*))$, and $s \equiv \text{sgn}(a_n)$. Define

$$\xi \equiv \left\{\frac{V_*}{2\pi|a_n|}\right\},$$

where $\{\cdot\}$ denotes the fractional part. This variable parametrizes different trajectories in the (γ,γ') plane (as well as on the torus τ_Φ in the physical space). In terms of ξ, we can write (20) as

$$\Delta\Phi = -2\sqrt{\varepsilon}s\pi\beta\cos(\pi z_*)\frac{c_n}{\sqrt{|a_n|}}$$

$$\times\int_{-s\infty}^{\gamma(t_*)}\frac{\cos\ \gamma}{\sqrt{2|s2\pi\xi + \gamma + (b_n/a_n)\sin\ \gamma|}}d\gamma + O(\varepsilon). \tag{21}$$

This analytical result is compared with the jump in the value of the AI computed by solving (1) numerically for $|b_n| > |a_n|$ in Fig. 5(a) and for $|b_n| < |a_n|$ in Fig. 5(b). In the former case, $\Delta\Phi(\xi)$ has a singularity at $\xi_{\text{sing}} = (2\pi)^{-1}\cos^{-1}(|a_n/b_n|)$ which corresponds to the trajectory passing near the hyperbolic fixed point in Fig. 4(a). It follows from (21) that the singularity is logarithmic. Therefore, there is a possibility (albeit quite small) of large jumps of Φ in the process of scattering.

For every set of initial conditions, the values of ξ and $\Delta\Phi$ can be calculated exactly. However, a small change $O(\varepsilon)$ in the initial conditions produces in general a large change $O(1)$ in ξ. Hence, for small ε, in computing the statistical properties of many consequent jumps, it is possible to treat ξ as a random variable uniformly distributed on the interval (0,1) (see Ref. [18]). The results of numerical integration of 2000 trajectories with initial conditions located in a small ball away from the resonance, presented in Fig. 6(a), confirm the uniform distribution of ξ. This allows us to readily evaluate

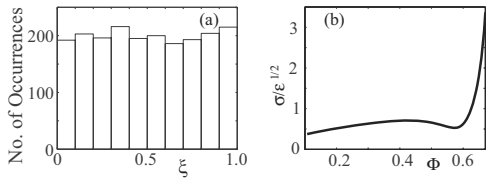

FIG. 6. Statistical properties of a single crossing of the 1:1 resonance for $\omega=2.5$, $\varepsilon=10^{-4}$, and $\beta=1$. (a) Histogram of the distribution of ξ. (b) Dispersion σ of the jump magnitude as a function of Φ before the jump.

the moments of the corresponding distribution of $\Delta\Phi(\xi)$. When $|b_n|>|a_n|$, the average value of the jump, $\langle\Delta\Phi\rangle$, is finite:

$$\langle\Delta\Phi\rangle = -s\sqrt{\varepsilon}\beta\cos(\pi z_*)\frac{c_n}{b_n}S, \tag{22}$$

where S is the area under the separatrix loop in Fig. 4(a):

$$S = \left|\int_{\gamma_0}^{\gamma_H}\sqrt{-2(V-V_H)}d\gamma\right|$$

where we have defined

$$V_H \equiv V(\gamma_H) = V(\gamma_0).$$

In the opposite case $|b_n|<|a_n|$, there is no separatrix, $S=0$, and hence $\langle\Delta\Phi\rangle=0$. Generally, a nonzero ensemble average of $\Delta\Phi$ results in a unidirectional drift of Φ. However, in the current problem, two successive crossings occur at almost the opposite values of z. Thus, they cancel each other *on average* because of the change of the sign of s, and the aggregate change of Φ on one period of the slow motion has zero mean. The second moment of $\Delta\Phi$,

$$\sigma^2 \equiv \int_0^1 (\Delta\Phi(\xi)-\langle\Delta\Phi\rangle)^2 d\xi = \sqrt{\varepsilon}f_n(\Phi), \tag{23}$$

is finite for any value of Φ. The function $f_n(\Phi)$ describes the dependence of the jump statistics on the value of Φ before the crossing [see Fig. 6(b)] and on the order n of the dominant resonance.

The dependence of $\Delta\Phi$ on the order of the resonance is determined by the scaling of a_n, b_n, and c_n, which are the Fourier coefficients of smooth functions (see Appendix A for details). In particular, a_n corresponds to the zeroth harmonic and increases linearly with n. On the other hand, b_n and c_n correspond to higher harmonics and decrease exponentially with n. As a consequence, the characteristic magnitude of the jumps decays exponentially. Thus, only low-order resonances contribute significantly to the change in the value of the AI. For high-order resonances,

$$\Delta\Phi \sim \sqrt{\varepsilon}e^{-\alpha n}, \tag{24}$$

where α is some constant. To illustrate (24), we computed the values of c_n—the most important factor in (21)—for several values of ω (chosen in such a way that the $1:n$ resonance surfaces R_n are located at the same location $\Psi=\Psi_n$ in the slow plane, which corresponds to the fixed value of $\Omega=2.5$). The results are presented in Table I. Only the values

TABLE I. The scaling of coefficients c_n with the order of the resonance.

n	c_n	n	c_n
1	-8.8×10^{-1}	7	-2.2×10^{-2}
3	-6.3×10^{-2}	9	-3.0×10^{-3}
5	-1.3×10^{-1}	11	-3.4×10^{-4}

for n odd are presented, as c_n vanishes identically for n even (see Appendix A). Note that the value of c_n is independent of ε and b.

B. Capture into resonance

It should be mentioned that under certain conditions a small fraction of tracers may be captured into resonance, i.e., follow trajectories that stay near the resonance surface for considerably longer periods of time compared with the case considered previously. It was shown in Ref. [13] that capture can be considered a probabilistic process: for a ball of initial conditions, only a small fraction of trajectories, of order $\sqrt{\varepsilon}$, are captured.

A typical trajectory experiencing capture is shown in Fig. 7. The captured dynamics is regular and possesses an AI which has nothing in common with Φ—the AI away from the resonance. Specifically, during capture tracers move near the cylinder $\Psi=\Psi_n$ [see Fig. 7(a)], so both Ψ and Ω, which is a function of Ψ, are essentially constant [see Fig. 7(b)]. Therefore, capture into resonance can be considered as a transition from one adiabatic-type motion to another.

In the physical space, captured trajectories are spirals near the resonant cylinder $\Psi(x,y)=\Psi_n$, with fast (period-T_n) rotation around the cylinder and slow $O(\varepsilon)$ drift in the positive (for $\Psi_n>\Psi_c$) or negative (for $\Psi_n<\Psi_c$) z direction. For the 1:1 resonance, the frequency of the fast rotation is almost the same as the frequency of the perturbation. Thus, a stroboscopic map (with the period $T_{st}=2\pi/\omega$) of the flow looks like a tight spiral, or even a one-dimensional (1D) curve [see

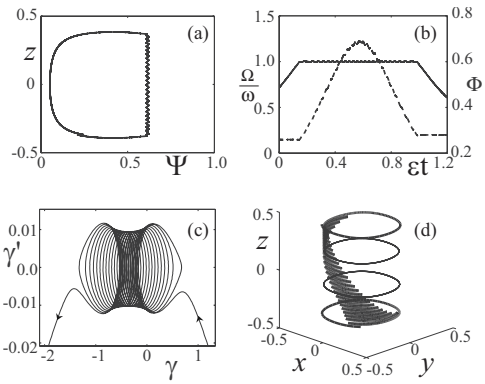

FIG. 7. Captured dynamics for $\varepsilon=b=10^{-4}$ and $\omega=2.5$. (a) Projection on (Ψ,z) plane. (b) Evolution of frequency Ω (solid line) and the AI Φ (dashed line) as a function of slow time. (c) Projection on the resonance (γ,γ') plane. (d) Stroboscopic map. Superimposed are two trajectories connecting successive iterates.

Fig. 7(d)]. To demonstrate that the trajectory is indeed a spiral, we also plotted a couple of coils connecting successive points of the stroboscopic map.

A more detailed description of the captured dynamics can be obtained by considering the evolution in the resonant (γ,γ') plane [see Fig. 7(c)]. One can see that the trajectory approaches the resonance (which corresponds to the γ axis) and leaves only after spending a significant amount of time in its vicinity. The captured trajectories are confined to the region inside the separatrix Σ as opposed to scattering on resonance, described by trajectories that pass outside the region inside Σ. Thus, at a given location, capture is possible if $|a_n|<|b_n|$ (the condition for the separatrix Σ to be present). Moreover, it can be shown that capture may not happen on every crossing, but only when $z_*<0$ for $\Psi_n>\Psi_c$ or $z_*>0$ for $\Psi_n<\Psi_c$. A more quantitative description of the captured dynamics is provided in Appendix B.

V. LONG-TERM DYNAMICS

A. Resonant processes and mixing

We have shown in the previous sections that, as a result of advection by the flow, an initially compact distribution of tracers [centered at a point (Ψ,z,χ)] is quickly stretched in one dimension to cover the streamline $\Gamma_{z,\Psi}$ on a time scale $O(1)$. Over a longer time scale $O(\varepsilon^{-1})$, the distribution is stretched over the whole level set $\tau_{\Phi(z,\Psi)}$ of the AI, becoming effectively two dimensional. In the absence of singular (e.g., resonance) manifolds, this is the greatest achievable degree of mixing.

It has long been recognized [4,5] that it is the spreading of the tracer distribution in the direction normal to the level sets $\tau_{\Phi(z,\Psi)}$ resulting from changes in the AI associated with resonant processes that is responsible for three-dimensional mixing. However, limited understanding of the resonant phenomena prevented any attempt at a quantitative description of the mixing dynamics. In fact, it was even unclear which of the resonant processes was responsible for the changes in the AI.

At first glance, it would appear that capture into resonance should have the most profound effect on the dynamics of the AI, which may change by $O(1)$ during captured motion, while scattering only changes the AI by $O(\sqrt{\varepsilon})$ (which is the scaling of the second moment of the distribution of the jumps). On the other hand, as we pointed out earlier, only a small fraction of trajectories, $O(\sqrt{\varepsilon})$, are captured, while the rest get scattered. Therefore, in a generic case, when the phase portrait of the averaged system possesses no special symmetry, in terms of the expectation values (the product of a characteristic magnitude of an event and its probability) capture and scattering play an equally important role in mixing (see, e.g, Ref. [11]). However, for the flow considered here, the trajectory is released at the value of z opposite to that at which it was captured (details are given in Appendix B). Hence, it follows from (11) that (in the first approximation) the values of Φ before and after capture are the same. Thus, in this particular problem capture provides a negligible contribution to the change in the AI and hence to the mixing dynamics.

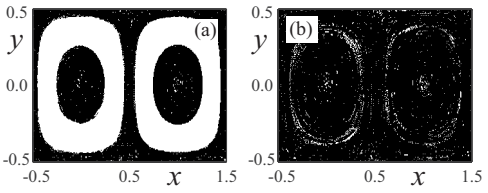

FIG. 8. Complete and partial mixing. $z=0$ Poincaré section of a single streamline with $\varepsilon=b=10^{-4}$ and $\omega=$ (a) 4.0 and (b) 2.5.

An alternative mixing mechanism (singularity-induced diffusion) proposed by Mezic [5] is based on changes in the value of the AI associated with passages through the vicinity of hyperbolic saddle- and saddle-focus-type periodic orbits with temporal period $T_{\mathrm{st}}=2\pi n/\omega$ (and their heteroclinic connections) surviving in the vicinity of the resonance surface for finite ε. Such periodic orbits would correspond to the hyperbolic fixed points $(\gamma_H,0)$ and the elliptic fixed point $(\gamma_E,0)$, respectively, in the resonant plane (see Fig. 4). However, periodic orbits would also have $\langle\dot{z}\rangle=0$ which, according to the discussion at the end of Sec. III B, is only possible for $z=\pm 0.5$ for the generic case $\Psi_n\neq\Psi_c$, so that periodic orbits would be confined to the top and bottom of the cell. Since very few trajectories ever pass near the very top and bottom of the resonance cylinder (and hence approach the periodic orbits and their heteroclinic connections), those heteroclinic connections cannot be responsible for mixing by this flow either.

Summing up, we find that it is the accumulation of many (mostly small) jumps of the AI associated with scattering on resonance that leads to chaotic advection, the adiabatic diffusion and, as a result, mixing in three dimensions [11]. The distribution of the AI, and hence the tracer distribution, broadens until eventually the whole chaotic domain is covered. Similarly to the case of steady flows in which adiabatic diffusion and mixing is due to separatrix crossings [19], two useful metrics can be introduced to provide a *global* description of chaotic advection and Lagrangian mixing: (1) the size (and shape) of the chaotic domain and (2) the characteristic rate of mixing inside the chaotic domain. We discuss these in turn below.

B. Volume of the mixed domain

On every period $T_\varepsilon(\Phi)$ of the slow motion along a given trajectory [see Fig. 2(b)], the value of Ψ changes between $\Psi_{\min}$ and $\Psi_{\max}$. If no (low-order) resonance Ψ_n falls in this interval, then that trajectory (and all trajectories inside it) remains regular. If, on the other hand, the trajectory crosses a resonance surface, the AI experiences jumps and the motion becomes chaotic.

In the $\varepsilon\to 0$ limit, the boundary between the chaotic and the regular domains is, thus, given by the trajectory Γ_{Φ^*} that (i) touches a resonance surface and (ii) has the largest value of Φ among all such trajectories on the (Ψ,z) plane [bold line in Fig. 2(b)]. Condition (ii) is necessary when multiple resonances are considered. In the physical space the boundary is formed by the corresponding torus τ_{Φ^*}. The Poincaré section of the complete flow by the plane $z=0$ [see Fig. 8(a)]

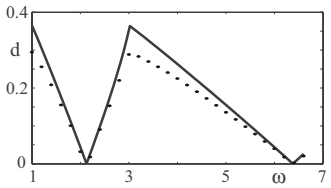

FIG. 9. Width d of the regular domain as a function of the perturbation frequency ω for $\varepsilon=b=10^{-4}$: solid line, theoretical prediction; dots, numerical simulations.

confirms that the space inside the torus τ_{Φ^*} corresponds to the regular domain discovered in Ref. [10], while the rest of the physical space belongs to the chaotic domain. Moving the frequency ω closer to the resonance with $\Omega(\Psi_c)\approx 2.2$ completely wipes out the regular domain [see Fig. 8(b)].

The width d of the regular domain can be computed easily for any value of ω (see Fig. 9). For $0<\omega\ll 1$, all the resonances are located near $\Psi=0$ (i.e., cell boundary). As ω is increased, the 1:1 resonance is the first to penetrate deeper into the cell. For $0<\omega\lesssim\pi$, Γ_{Φ^*} is tangent to the resonance $\Psi=\Psi_1$ [see Fig. 2(b)]. As ω approaches π, the 1:1 resonance is pushed out of the cell and the 1:3 resonance becomes the most prominent for $\pi\lesssim\omega\lesssim 3\pi$ (recall that even resonances do not lead to jumps in Φ and thus do not contribute to adiabatic diffusion). Then the process repeats itself: as ω is increased further, low-order resonances are pushed out of the cell and higher resonances become prominent. Finally, as $\omega\to\infty$, the cell becomes uniformly covered by high-order resonances. However, the impact of the high resonances is exponentially small and hence we can expect mixing to become spatially uniform only on exponentially long time scales. On finite time scales characteristic of experiments (e.g., those reported in Ref. [10]), it would appear that no mixing is taking place in three dimensions. We should also point out that, for the flow between concentric spheres considered in Refs. [1,4], complete mixing relies on high-order resonances and, while conceptually possible, would similarly require exceedingly long times.

In our case, complete mixing on experimentally accessible time scales can be achieved by eliminating the domain of regular dynamics via a proper placement of a low-order resonance. This can be accomplished by setting the frequency ω of the perturbation such that $\Psi_n(\omega)=\Psi_c$ for some n. More precisely, the resonance must be within the interval $|\Psi_n-\Psi_c|=O(\sqrt{\varepsilon})$, as the chaotic domain penetrates inside Γ_{Φ^*} by a distance $O(\sqrt{\varepsilon})$ [20]. This property, negligible in most similar problems, is important here as the magnitude of the jumps vanishes at Ψ_c. Indeed, $\dot{\Phi}\sim\dot{z}$ according to (19), so $\Delta\Phi=0$ at $\Psi=\Psi_c$, as $\dot{z}=0$ there. Since the width of the regular domain $d\sim|\Psi_n(\omega)-\Psi_c|$, we find the width of the frequency intervals yielding complete mixing (where $d\approx 0$) to scale as $\Delta\omega\sim\sqrt{\varepsilon}$ (see Fig. 9).

C. Characteristic time of mixing

Formal definition of the regular and chaotic domains assumes evolution over an infinite time. However, any particular experiment is characterized by a finite time interval. While the evolution inside the regular domain remains qualitatively the same, the thoroughness of mixing in the chaotic domain (as well as the mixed volume fraction) depends on the time interval of observation.

Quantitative properties of the diffusion of the AI depend on statistical properties of the resonance phase ξ. As we argued previously, for a single crossing the values of ξ can be considered a random variable uniformly distributed on the interval (0,1). Using the ergodicity assumption, we can deduce the same property for any given long-time trajectory. Furthermore, it can be shown that consecutive crossings are statistically independent. Statistical independence follows from the divergence of phases ξ along trajectories and, for Hamiltonian systems, was demonstrated in Ref. [18]. In volume-preserving systems, it can be confirmed following similar lines (see also [21]).

Using statistical independence of consecutive crossings, we can estimate the rate of mixing. The evolution of Φ can be considered a random walk with a characteristic step size $\Delta\Phi$. A characteristic time of mixing can be defined as the time needed for a δ-localized distribution of initial conditions with $\Phi=\Phi_0$ to diffuse over the entire chaotic domain. For small times t, the width of the distribution inside the chaotic domain (and hence the mixed volume fraction) grows as $\sigma N^{1/2}$, where $N(\Phi)=2t/T_\varepsilon(\Phi)$ is the number of resonance crossings, $T_\varepsilon(\Phi)=O(\varepsilon^{-1})$ is the period of motion around Γ_Φ, and $\sigma(\Phi)=\sqrt{\varepsilon}f_n(\Phi)$ is the dispersion of $\Delta\Phi$ over one crossing. As we have shown in Sec. IV A, $f_n(\Phi)$ takes $O(1)$ values for n small and decreases exponentially with increasing n for n large. It takes $N\sim\bar{\sigma}^{-2}$ resonance crossings for the distribution to diffuse over the entire chaotic domain, where $\bar{\sigma}$ is a weighted average of $\sigma(\Phi)$ which can be computed analytically (to be discussed in more detail in a subsequent presentation). Therefore, the characteristic time of mixing

$$T_M\sim T_\varepsilon N=O(\varepsilon^{-2}e^{2\alpha n}) \tag{25}$$

diverges, while the rate of mixing, defined as $1/T_M$, vanishes, as either $\varepsilon\to 0$ or $n\to\infty$. A similar result was reported in Ref. [3].

A more accurate estimate can be obtained by including the contributions to the adiabatic dispersion from all the resonances that a given trajectory crosses. As only the low-order resonances contribute significantly and they are far apart, their effect may be considered independently. Moreover, the contributions of different low-order resonances can vary considerably with the resonance order (e.g., only odd resonances contribute to the flow considered here) and with the value of Ψ_n (e.g., the jumps near $\Psi_n=\Psi_c$ are strongly suppressed), so additional simplifications are possible.

D. Mixing uniformity

Although this was not our focus here, one could obtain a more quantitative description of the mixing *uniformity* inside the chaotic domain, e.g., as a function of time. It is known [22] that the chaotic region may contain small regular islands of size $\delta=O(\varepsilon)$. Our analysis shows that the tracer distribution will be uniform at length scales larger than δ at long

times (asymptotically); however, nonuniformity can still be found at smaller length scales or shorter times. This (non-)uniformity can be represented, for instance, in terms of the length-scale-sensitive mix norms [23].

We should also point out that popular characteristics of mixing based on the introduction of a Poincaré section (see, e.g., [24]) provide a poor description of mixing properties of weakly perturbed flows at short times due to the presence of very long $[O(\varepsilon^{-1})$ or longer] time scales. A more efficient description can be provided, at least on length scales larger than δ, in terms of an effective diffusion equation describing the long-time evolution of the probability density function of the AI, which can be derived using the second moment given by (23). This latter approach is currently under investigation.

VI. CONCLUSIONS

In summary, we have confirmed that Lagrangian mixing in the periodically driven near-integrable cellular flow introduced by Solomon and Mezic [10] is due to the accumulation of (mostly small) changes experienced by an adiabatic invariant of the flow when the streamlines cross the surfaces on which the perturbation frequency is in resonance with the natural frequency of the unperturbed flow, confirming the resonance-induced adiabatic diffusion mechanism proposed by Feingold and co-workers [2,3]. In particular, we have shown that the mechanism proposed by Mezic [5] does not contribute appreciably to the adiabatic diffusion. Moreover, we have shown that capture into resonance [13] associated with large changes in the AI does not contribute to mixing in this flow either.

We have constructed a quantitative theory predicting the magnitude of the jumps experienced by the adiabatic invariant upon crossing resonance surfaces which, when combined with the statistics of the crossing events, can be used to quantitatively describe adiabatic diffusion and mixing on long time scales. Finally, the nonmonotonic dependence of the mixed volume on the frequency of the perturbation discovered in Ref. [10] was traced to the dependence of the position of the resonance surfaces on the perturbation frequency. In particular, we have shown that different low-order resonances (e.g., 1:1 or 1:3) can be used to achieve essentially complete mixing inside the cell on experimentally accessible time scales.

ACKNOWLEDGMENTS

This paper is based upon work supported by the NSF under Grant No. 0400370. Acknowledgment is also made to the Donors of the ACS Petroleum Research Fund, for partial support of this research. D.V. is grateful to the Russian Basic Research Foundation Grant No. 06-01-00117. We are also grateful for useful discussions with A.I. Neishtadt and A.A. Vasiliev.

APPENDIX A

Here we derive the leading-order expansions for b_n and c_n near the resonance. To compute these, we need to find the following averages over the fast period:

$$\langle f(\chi)\sin(\omega t)\rangle_{T_n} = \frac{1}{2\pi}\int_0^{2\pi} f(\chi)\sin(\omega t)d\chi,$$

where $f(\chi)=f(x(t(\chi)),y(t(\chi)))$ denotes one of two functions:

$$f(x,y) = \begin{cases} \sin(2\pi y), \\ [\cos(2\pi x)+\cos(2\pi y)]\sin(2\pi y). \end{cases}$$

In the above averages, $x=x(t)$ and $y=y(t)$ is the solution of the unperturbed system for $\Psi=\Psi_n$ such that $n\chi=\gamma$ at $t=0$.

In both cases, $f(-\chi)=-f(\chi)$ and $f(\pi+\chi)=-f(\chi)$. Therefore, in the Fourier expansion

$$f(\chi) = \sum_m g_m \sin(m\chi) \tag{A1}$$

there are no $\cos(m\chi)$ terms and only odd-m terms are present. Multiplying both sides of (A1) by $\sin(\omega t)$ and integrating over one period in χ, we get in the leading approximation

$$\int_0^{2\pi} f(\chi)\sin(\omega t)d\chi = \int_0^{2\pi}\sum_m g_m \sin(m\chi)\sin(\omega t)d\chi$$

$$= \frac{1}{2}g_n \cos\gamma,$$

where n is the resonant term, as all nonresonant terms average out. For g_n we have

$$g_n(\omega) = \frac{1}{\pi}\int_0^{2\pi} f(\chi)\sin n\chi\, d\chi. \tag{A2}$$

Substituting (A2) into (17) and (19), we obtain the expressions for b_n and c_n.

APPENDIX B

The relative magnitude of a_n and b_n defined by (18) determines both the possibility of capture into resonance and the structure of the phase space that corresponds to captured dynamics. At a given location on the resonance surface, capture is possible only if $|b_n/a_n|>1$. For fixed values of ω and n, the ratio b_n/a_n depends only on the value of β and the location of the crossing, z_*, as $a_n=a_n(z_*)=\bar{a}_n\sin(\pi z_*)$ and $b_n=\bar{b}_n\beta$, with $\bar{a}_n$ and $\bar{b}_n$ some constants. Since $a_n=0$ at $z=0$, capture is always possible near the z axis, inside the domain $(-z_{\max},z_{\max})$ whose width depends on the value of β. If $|b_n/\bar{a}_n|<1$, we have $z_{\max}=\sin^{-1}(|b_n/\bar{a}_n|)/\pi$. If $|b_n/\bar{a}_n|\geq 1$, we have $z_{\max}=1/2$, so that capture can happen anywhere on the resonance surface R_n.

As the captured trajectory drifts along R_n, the value of Ψ is fixed, but z slowly changes and hence the phase portrait also slowly changes. In particular, for $|z|<z_{\max}$ the phase portrait looks like the one in Fig. 4(a). There are two fixed points on the (γ,γ') plane—an elliptic point $(\gamma_E,0)$ and a hyperbolic point $(\gamma_H,0)$—and a separatrix Σ. As $|z|$ approaches $z_{\max}$ the separatrix shrinks to a point, the fixed points merge, and all of them disappear for $|z|>z_{\max}$, where the phase portrait looks like the one in Fig. 4(b).

The captured motion is described by a trajectory confined inside the separatrix Σ and possesses an additional AI Θ (see

Ref. [13]). This invariant is defined as the area enclosed by a trajectory during one revolution in the (γ,γ') plane [one coil in Fig. 7(c)] or, equivalently, as the area inside the corresponding level set of the resonance Hamiltonian

$$H(\gamma,\gamma') = \frac{1}{2}\gamma'^2 + V(\gamma). \tag{B1}$$

For a given captured trajectory, the value of Θ is equal to the area $S(z_*)$ under the separatrix Σ at the moment of capture. $S(z)$ is an even function of z that achieves its maximum at $z=0$ and its minimum $S_{\min}$ at $\pm z_{\max}$, and which is monotonic on the intervals $(-z_{\max},0)$ and $(0,z_{\max})$. Hence, after the trajectory has been captured, Θ stays constant, while $S(z)$ first increases and then, after the z axis is crossed, starts to decrease. Once $S(z)$ becomes once again equal to Θ, the trajectory crosses the separatrix and is released from resonance. The conservation of Θ, therefore, relates the values of z at which the trajectory is released from, and captured into, the resonance: to leading order, the trajectory is released at $z=-z_*$.

Furthermore, it can be shown that, $S_{\min}=0$ for $z_{\max}<1/2$ and $S_{\min}>0$ for $z_{\max}=1/2$. Since during the captured motion Θ is bounded by $S_{\min}$ from below, for $|b_n/\bar{a}_n|\geq 1$ no trajectory can be captured into the resonance with $\Theta<S_{\min}$. Therefore, for every z, the level set of (B1) corresponding to $\Theta=S_{\min}$ defines the boundary of an "excluded" domain that is separated from the rest of the plane. No trajectories ever enter the excluded domain from outside and no trajectories ever leave the excluded domain. Every trajectory found inside the excluded domain has initial conditions inside that domain. The larger is the value of β, the larger the excluded domain.

The captured motion has the same separation of scales as the adiabatic motion; namely, the (x,y) motion is fast and the evolution on the (Ψ,z) plane is slow. Thus, captured motion, regardless of the value of Θ, looks like a spiral on the "thick" cylinder $\Psi\approx\Psi_n(\omega)$. The smaller is the value of Θ, the closer is the projection of the corresponding trajectory on the (γ,γ') plane to the elliptic point γ_E and the smaller is the thickness of the cylinder [defined as the maximum distance from the resonant cylinder $\Psi=\Psi_n(\omega)$, or equivalently, the amplitude of the waving in Fig. 7(a)]. However, the size of the (x,y) oscillations is almost independent of the value of Θ.

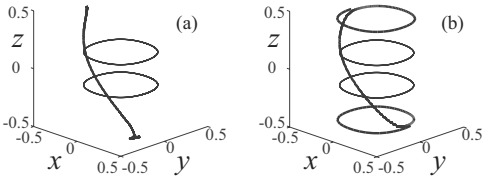

FIG. 10. Stroboscopic (with the period $T_{st}=2\pi/\omega$) map of captured trajectories near the elliptic fixed point on the resonance plane with $\varepsilon=b=10^{-4}$ and $\omega=2.5$. Trajectory in (a) and outside (b) the excluded domain.

A typical captured motion near $(\gamma_E,0)$ for the 1:1 resonance is illustrated in Fig. 10. The thick lines on both panels show the iterates of a stroboscopic map with the period $T_{\rm st}=2\pi/\omega$. Right on R_1, $T_{\rm st}$ is exactly equal to the period of the (x,y) motion. As a result, a stroboscopic map of a spiral looks like a 1D curve in Fig. 10. To illustrate that the trajectory is indeed a spiral, we plotted a couple of coils between the subsequent points of the stroboscopic map. The curve in Fig. 10(a) corresponds to the excluded domain. The trajectory stretches from $z=-1/2$ to $z=1/2$ and, upon coming to $z=1/2$, stays there. This trajectory is similar to the one presented in Fig. 2(c) in [10] and corresponds to a heteroclinic connection between two periodic orbits, one at the top and one at the bottom surface of the cell. On the other hand, Fig. 10(b) shows the captured motion for parameters at which there is no excluded domain, with the trajectory captured and released at $z\approx\pm 0.44$. Before and after the release the trajectory corresponds to regular adiabatic motion near the top and bottom of the cell.

[1] J. H. E. Cartwright, M. Feingold, and O. Piro, J. Fluid Mech. **316**, 259 (1996).
[2] M. Feingold, L. P. Kadanoff, and O. Piro, J. Stat. Phys. **50**, 529 (1988).
[3] O. Piro and M. Feingold, Phys. Rev. Lett. **61**, 1799 (1988).
[4] J. H. E. Cartwright, M. Feingold, and O. Piro, Phys. Rev. Lett. **75**, 3669 (1995).
[5] I. Mezic, Physica D **154**, 51 (2001).
[6] A. J. S. Rodrigo, J. P. B. Mota, A. Lefevre, J. C. Leprevost, and E. Saatdjian, AIChE J. **49**, 2749 (2003).
[7] T. Ward and G. M. Homsy, Phys. Fluids **15**, 2987 (2003).
[8] R. Chabreyrie, D. Vainchtein, C. Chandre, P. Singh, and N. Aubry, Phys. Rev. E **77**, 036314 (2008).
[9] B. R. Noack, I. Mezic, G. Tadmor, and A. Banaszuk, Phys. Fluids **16**, 867 (2004).
[10] T. H. Solomon and I. Mezic, Nature (London) **425**, 376 (2003).
[11] D. L. Vainchtein, A. I. Neishtadt, and I. Mezic, Chaos **16**, 043123 (2006).
[12] D. L. Vainchtein, J. Widloski, and R. O. Grigoriev, Phys. Rev. Lett. **99**, 094501 (2007).
[13] A.I. Neishtadt, Proc. Steklov Inst. Math. **250**, 183 (2005).
[14] D. L. Vainshtein, A. A. Vasiliev, and A. I. Neishtadt, Chaos **6**, 67 (1996).
[15] L. S. Gradshtein and I. M. Ryzhik, *Tables of Sums, Integrals and Series* (Academic, Boston, 1994).
[16] R. Bachelard, T. Benzekri, C. Chandre, X. Leoncini, and M. Vittot, Phys. Rev. E **76**, 046217 (2007).
[17] M.A. Fogleman, M.J. Fawcett, and T.H. Solomon, Phys. Rev. E **63**, 020101(R) (2001).
[18] A. I. Neishtadt, in *Hamiltonian Systems with Three or More Degrees of Freedom,* edited by C. Simó, NATO Advanced Studies Institute, Series C: Mathematical and Physical Sciences (Kluwer Acacemic, Dordrecht, 1999), Vol. 533, pp. 193–213.
[19] D. L. Vainchtein, J. Widloski, and R. O. Grigoriev, Phys. Flu-

ids **19**, 067102 (2007).
[20] D. L. Vainshtein, A. A. Vasiliev, and A. I. Neishtadt, Chaos **6**, 514 (1996).
[21] D. Dolgopyat, University of Maryland report, 2004 (unpublished).
[22] A. I. Neishtadt, C. Simó, D. V. Treschev, and A. A. Vasiliev, Discrete Contin. Dyn. Syst., Ser. B (to be published).
[23] G. Mathew, I. Mezic, and L. Petzold, Physica D **211**, 23 (2005).
[24] M. Funakoshi, Fluid Dyn. Res. **40**, 1 (2008).